Crystal Growth, Structure, and Physical Properties of Ln_2MGa$_{12}$ (Ln = La, Ce; M = Ni, Cu)

Jung Young Cho,[†] Jasmine N. Millican,[†,‡] Cigdem Capan,[§] Dmitry A. Sokolov,[||] Monica Moldovan,[§] Amar B. Karki,[§] David P. Young,[§] Meigan C. Aronson,[||,⊥] and Julia Y. Chan*[,†]

Department of Chemistry and Department of Physics and Astronomy, Louisiana State University, Baton Rouge, Louisiana 70803, NIST Center for Neutron Research, National Institute of Standards and Technology, Gaithersburg, Maryland 20899, Brookhaven National Laboratory, Upton, New York 11973, and Department of Physics and Astronomy, State University of New York, Stony Brook, New York 11794

Received June 20, 2008. Revised Manuscript Received July 11, 2008

Single crystals of Ln_2MGa$_{12}$ (Ln = La, Ce; M = Ni, Cu) have been synthesized using Ga flux and their structures determined by single-crystal X-ray diffraction. The Ln_2MGa$_{12}$ (Ln = La, Ce; M = Ni, Cu), which is isostructural to Ce$_2$PdGa$_{12}$, crystallizes in the tetragonal *P*4/*nbm* (No. 125, origin choice 2) space group, with $Z = 2$ and lattice parameters $a \approx 6.1$ Å and $c \approx 15.3$ Å. Ce$_2$NiGa$_{12}$ orders antiferromagnetically at 10 K and specific heat measurements suggest it is a moderate heavy-fermion system with $\gamma \approx 191$ mJ mol^{-1} K^{-2}. Magnetic susceptibility data show paramagnetic behavior down to 2 K for Ce$_2$CuGa$_{12}$, whereas specific heat data suggest a magnetic transition below 1.8 K, with a moderately enhanced γ-value of 69 mJ mol^{-1} K^{-2}. Metallic behavior is observed below 300 K for each compound. A large positive and nonsaturating magnetoresistance up to 216% at a field (μ_0H) of 9 T is also observed for La$_2$NiGa$_{12}$. We present the crystal structures and physical properties of the Ln_2MGa$_{12}$ (Ln = La, Ce; M = Ni, Cu) series.

Introduction

Ce-containing heavy-fermion ternary compounds, which show large electronic masses ($m^* \approx 100-1000\ m_e$), have been of interest because of their exotic physical properties, such as magnetic ordering and superconductivity.[1−4] In these systems there is a competition between the tendency toward magnetic order of *f*-electrons via hybridization pathways with the conduction electrons (RKKY mechanism) and the tendency toward the screening of magnetic moments (Kondo effect) producing large effective electron masses. Recently the structure and properties of Ce$_2$PdGa$_{12}$ and CePdGa$_6$ have been reported.[5] CePdGa$_6$ consists of alternating layers of CeGa$_{8/4}$ and PdGa$_{8/2}$ in a 1:1 ratio, and in contrast Ce$_2$PdGa$_{12}$ consists of Ce bilayers including Ga-only segments and single layers of CuGa$_{8/2}$ along the crystallographic *c*-axis.[5] In the case of Ce$_2$PdGa$_{12}$, the bilayer structure seems to favor magnetic ordering mediated by RKKY, in contrast to the single Ce layered compound, which tends to favor Kondo behavior with enhanced quasiparticle mass. Also, CeCoIn$_5$ has been reported as a heavy-fermion compound (Sommerfeld coefficient of specific heat, $\gamma \approx 500$ mJ mol^{-1} K^{-2}), which also shows a superconducting transition temperature ($T_c = 2.3$ K) at ambient pressure.[6] The superconductivity in this family of compounds Ce$_n M$In$_{3n+2}$ ($n = 1$) is unusual, in that it tends to coexist with static magnetism. Also, the related compounds, Ce$_2M$In$_8$ (M = Co, Rh, and Ir), exhibit heavy-fermion behavior with $\gamma \approx 500$, 400, and 700 mJ mol^{-1} K^{-2} for the Co-, Rh-, and Ir-containing compounds, respectively.[7−9] Although various experiments have been performed on many systems in this interesting class of compounds, a comprehensive understanding of heavy-fermion properties at low temperature is still lacking.

We have synthesized Ln_2MGa$_{12}$ (Ln = La, Ce; M = Ni, Cu), which are isomorphous to Ce$_2$PdGa$_{12}$.[5] Our major interest in investigating these materials lies with the fact that Ce-based heavy fermion superconductors at ambient pressure are very rare. The original heavy fermion superconductor,

* To whom correspondence should be addressed. E-mail: jchan@lsu.edu. Phone: (225) 578-2695. Fax: (225) 578-3458.
[†] Department of Chemistry, Louisiana State University.
[‡] National Institute of Standards and Technology.
[§] Department of Physics and Astronomy, Louisiana State University.
[||] Brookhaven National Laboratory.
[⊥] State University of New York.

(1) Fisk, Z.; Hess, D. W.; Pethick, C. J.; Pines, D.; Smith, J. L.; Thompson, J. D.; Willis, J. O. *Science* **1988**, *239*, 33–42.
(2) Stewart, G. R. *Rev. Mod. Phys.* **1984**, *56*, 755–787.
(3) Fisk, Z.; Sarrao, J. L.; Thompson, J. D. *Curr. Opin. Solid State Mater. Sci.* **1996**, *1*, 42–46.
(4) Fisk, Z.; Sarrao, J. L.; Smith, J. L.; Thompson, J. D. *Proc. Natl. Acad. Sci. U.S.A.* **1995**, *92*, 6663–6667.
(5) Macaluso, R. T.; Millican, J. N.; Nakatsuji, S.; Lee, H.-O.; Carter, B.; Moreno, N. O.; Fisk, Z.; Chan, J. Y. *J. Solid State Chem.* **2005**, *178*, 3547–3553.
(6) Petrovic, C.; Pagliuso, P. G.; Hundley, M. F.; Movshovich, R.; Sarrao, J. L.; Thompson, J. D.; Fisk, Z.; Monthoux, P. *J. Phys.: Condens. Matter* **2001**, *13*, L337−L342.
(7) Macaluso, R. T.; Sarrao, J. L.; Moreno, N. O.; Pagliuso, P. G.; Thompson, J. D.; Fronczek, F. R.; Hundley, M. F.; Malinowski, A.; Chan, J. Y. *Chem. Mater.* **2003**, *15*, 1394–1398.
(8) Nicklas, M.; Sidorov, V. A.; Borges, H. A.; Pagliuso, P. G.; Petrovic, C.; Fisk, Z.; Sarrao, J. L.; Thompson, J. D. *Phys. Rev. B: Condens. Matter* **2003**, *67*, 020506/1–020506/4.
(9) Hedo, M.; Kurita, N.; Uwatoko, Y.; Chen, G.; Ohara, S.; Sakamoto, I. *J. Magn. Magn. Mater* **2004**, *272−276*, 146–147.

10.1021/cm801693t CCC: $40.75
Published on Web 09/06/2008

$CeCu_2Si_2$, was the only example until very recently.[10] Searching chemical phase space allows the opportunity to discover other intermetallic Ce compounds that share similar physical properties to $CeCu_2Si_2$ and Ce_nMIn_{3n+2}. If this new class of compounds is found to superconduct, at ambient pressure or otherwise, the presence of strong magnetic interactions between the 4*f* levels and itinerant electrons inherent in these systems, may give rise to unconventional superconductivity, where the pairing mechanism is mediated by something other than phonons.

These structures can be viewed as a three-dimensional network of [*M*Ga] (*M* = Cu, Ni) with Ce atoms occupying cavities made of Ga atoms. In this paper, we compare the structures of Ce_2MGa_{12} (*M* = Ni, Cu) and Ce_2PdGa_{12} and investigate the role of the transition metal environments as they relate to the physical properties of these compounds. A partial contribution to the total electron DOS, which refers to the total number of available states for occupation at each energy level, at the Fermi surface from the transition metal has been suggested by band structure calculations of Sm_2NiGa_{12}.[11] By substituting Cu for Ni, we would expect to change the electronic properties. The properties of the Ce_nMIn_{3n+2} family of compounds are intimately tied to the choice of the transition metal. In previous studies, a change in γ has been observed to occur when Pd is substituted by Cu or Ni. For example, the heavy-fermion $CePd_2Si_2$[12,13] has a $\gamma \approx 250$ mJ mol^{-1} K^{-2}, whereas the isostructural Cu analogue[10,14] shows enhanced electron mass with $\gamma \approx 1100$ mJ mol^{-1} K^{-2}. Several other copper-containing compounds such as $CeCu_4Al$, $CeCu_3Al_2$, and $CeCu_4Ga$ also show heavy-fermion behavior with $\gamma \approx 1000$ mJ mol^{-1} K^{-2}, 490 mJ mol^{-1} K^{-2}, and 3000 mJ mol^{-1} K^{-2}, respectively.[15−17]

Experimental Section

Synthesis. Single crystals of Ln_2MGa_{12} (*Ln* = La, Ce; *M* = Ni, Cu) were prepared by gallium flux growth method. La or Ce ingot (3N, Ames Laboratory), Cu or Ni powder (5N, Alfa Aesar), and Ga (6N, Alfa Aesar) were placed into alumina crucibles in a 1.5:1:15 ratio. The crucible containing the starting materials was then sealed into an evacuated fused silica tube and heated up to 1423 K at a rate of 170 K/h and allowed to dwell for 7 h at that temperature. After fast cooling at a rate of 150 K/h to 773 K, the fused silica tube was allowed to cool slowly to 673 K at a rate of 8 K/h and immediately inverted and centrifuged. Silver-colored plate-like aggregates of crystals were found and mechanically separated from gallium flux. Typical crystal size ranged from 1 × 2 × 2 to 1 × 2 × 5 mm^3. The crystals were stable in air. Single crystals from several growths of La_2CuGa_{12} were ground for powder neutron experiment.

Powder and Single-Crystal X-ray Diffraction. Silver-colored fragments (≈ 0.01 mm × 0.01 mm × 0.01 mm to 0.03 mm × 0.03 mm × 0.05 mm) of La_2NiGa_{12} and Ce_2MGa_{12} (*M* = Ni, Cu) were attached on a thin glass fiber using a two-component adhesive and mounted onto the goniometer of a Nonius KappaCCD diffractometer equipped with a Mo Kα radiation ($\lambda = 0.71073$ Å) X-ray tube. Single crystal data were collected at 298 K for all samples, and additional data were collected at 90 K to examine disorder in Ce_2CuGa_{12}. Direct methods were used to solve the structure. SHELXL97 was used to refine the structural model of the La_2NiGa_{12} and Ce_2MGa_{12} (*M* = Ni, Cu) compounds, and data were corrected with extinction coefficients and refined with anisotropic displacement parameters. The obtained structural model was compared to the crystallographic data from Sm_2NiGa_{12}. Crystallographic parameters for La_2NiGa_{12} and Ce_2MGa_{12} (*M* = Ni, Cu) are provided in Table 1. Atomic positions and displacement parameters for the compounds are given in Table 2, and selected interatomic distances are also provided in Table 3. Powder X-ray diffraction data were collected on several ground single crystals of each compound to examine the phase purity. The diffraction patterns show peaks that are consistent with their calculated powder patterns. Although the single crystals of La_2CuGa_{12} were not of sufficient quality and the structure could not be confirmed using single-crystal X-ray diffraction experiments, powder X-ray diffraction techniques were used to index the pattern of La_2CuGa_{12} as isostructural to the analogous 2−1−12 phases. Neutron powder diffraction experiments were ultimately used to solve the structure of La_2CuGa_{12}. Additional crystallographic parameters, atomic positions, and interatomic distances for La_2CuGa_{12} are also provided in Tables 1−3.

Neutron Powder Diffraction (NPD). A 3.71 g powder sample of La_2CuGa_{12} was loaded in a vanadium container of length 50 mm and diameter 6.0 mm. Neutron powder diffraction data were collected using the BT-1 32 detector neutron powder diffractometer at the NIST Center for Neutron Research (NCNR). A Cu(311) monochromator with a 90° takeoff angle, $\lambda = 1.5403(2)$ Å, and in-pile collimation of 15′ of arc were used. Data were collected over the range of 3° to 166° 2θ with a step size of 0.05° under ambient conditions. Rietveld refinement of the structure of La_2CuGa_{12} was performed using the GSAS software package with the EXPGUI interface.[18,19]

Physical Property Measurements. Magnetic data were obtained using a Quantum Design physical property measurement system (PPMS). The temperature-dependent susceptibility data were obtained under zero-field cooled (ZFC) conditions from 2 to 300 K under an applied field ($\mu_0 H$) of 0.1 T, and then measured upon heating to obtain field-cooled (FC) data after cooling to 2 K under field. Field-dependent magnetization data were measured at 3 K with field ($\mu_0 H$) up to 9 T. The electrical resistivity and magnetoresistance (MR) were measured by the standard four-probe AC technique. Measurements of the heat capacity were performed using a Quantum Design physical property measurement system at temperatures from 0.35 to 70 K.

Results and Discussion

Structure. The structure of Ce_2CuGa_{12} is shown in Figure 1. Ce_2MGa_{12} (*M* = Ni, Cu), which are isostructural to Sm_2NiGa_{12}[11] and Ce_2PdGa_{12},[5] crystallize in the tetragonal

(10) Steglich, F.; Aarts, J.; Bredl, C. D.; Lieke, W.; Meschede, D.; Franz, W.; Schaefer, H. *Phys. Rev. Lett.* **1979**, *43*, 1892–1896.
(11) Chen, X. Z.; Small, P.; Sportouch, S.; Zhuravleva, M.; Brazis, P.; Kannewurf, C. R.; Kanatzidis, M. G. *Chem. Mater.* **2000**, *12*, 2520–2522.
(12) Mathur, N. D.; Grosche, F. M.; Julian, S. R.; Walker, I. R.; Freye, D. M.; Haselwimmer, R. K. W.; Lonzarich, G. G. *Nature* **1998**, *394*, 39–43.
(13) Grier, B. H.; Lawrence, J. M.; Murgai, V.; Parks, R. D. *Phys. Rev. B* **1984**, *29*, 2664.
(14) Steglich, F. *Physica B* **2005**, *359−361*, 326–332.
(15) Bauer, E.; Gignoux, D.; Schmitt, D.; Winzer, K. *J. Magn. Magn. Mater.* **1987**, *69*, 158–162.
(16) Dhar, S. K.; Gschneidner, K. A., Jr. *J. Magn. Magn. Mater.* **1989**, *79*, 151–153.
(17) Bauer, E.; Pillmayr, N.; Gratz, E.; Gignoux, D.; Schmitt, D.; Winzer, K.; Kohlmann, J. *J. Magn. Magn. Mater.* **1988**, *71*, 311–17.
(18) Larson, A. C.; Von Dreele, R. B. *GSAS−Generalized Structure Analysis System*; LANSCE, MS-H805; Los Alamos National Laboratory: Los Alamos, NM, 2000.
(19) Toby, B. H. *J. Appl. Crystallogr.* **2001**, *34*, 210–213.

Table 1. Crystallographic Parameters

Crystal Data					
formula	La_2NiGa_{12}	Ce_2NiGa_{12}	La_2CuGa_{12}	Ce_2CuGa_{12} (298 K)	Ce_2CuGa_{12} (90 K)
cryst syst	tetragonal	tetragonal	tetragonal	tetragonal	tetragonal
space group	*P4/nbm*	*P4/nbm*	*P4/nbm*	*P4/nbm*	*P4/nbm*
a (Å)	6.073(3)	6.036(2)	6.1760(1)	6.108(3)	6.090(2)
c (Å)	15.547(5)	15.506(8)	15.3660(3)	15.375(4)	15.348(7)
V (Å^3)	573.4(4)	564.9(4)	586.11(3)	573.6(4)	569.2(4)
Z	2	2	2	2	2
cryst dimension (mm^3)	0.03 × 0.03 × 0.05	0.05 × 0.05 × 0.08		0.05 × 0.05 × 0.08	0.03 × 0.05 × 0.05
2θ range (deg)	5.24−60.06	9.56−60.02	3.0−167.8	7.96−59.96	7.96−60.14
μ (mm^{-1})	36.474	37.516		37.161	37.447
Data Collection					
no. of measured reflns	1449	1120		1455	1259
no. of independent reflns	480	456		481	476
reflns with $I > 2\sigma(I)$	417	375		423	375
R_{int}	0.0310	0.0307	0.0310	0.0504	0.0413
h	−8 → 8	−8 → 8	0 → 8	−8 → 8	−8 → 8
k	−6 → 6	−6 → 6	0 → 5	−6 → 6	−5 → 6
l	−20 → 21	−21 → 11	0 → 19	−21 → 20	−16 → 21
Refinement					
no. of reflns	480	456	3296	481	476
params	26	26	52	26	26
[a] R_1 [$F^2 > 2\sigma(F^2)$]	0.0272	0.0298	0.0402	0.0558	0.0433
[b] wR_2 (F^2)	0.0632	0.0627	0.0657	0.1444	0.1045
$\Delta\rho_{max}$ (e Å^{-3})	2.164	2.485		6.689	5.635
$\Delta\rho_{min}$ (e Å^{-3})	−1.546	−1.396		−9.427	−3.352

[a] $R_1 = \sum||F_o| - |F_c||/\sum|F_o|$. [b] $wR_2 = [\sum[w(F_o^2-F_c^2)]/\sum[w(F_o^2)^2]]^{1/2}$, $w = 1/[\sigma^2(F_o^2) + (0.0252P)^2 + 4.0550P]$ for La_2NiGa_{12}, $w = 1/[\sigma^2(F_o^2) + (0.0222P)^2 + 2.0096P]$ for Ce_2NiGa_{12}, $w = 1/[\sigma^2(F_o^2) + (0.0775P)^2 + 11.6928P]$ for Ce_2CuGa_{12} (298 K), $w = 1/[\sigma^2(F_o^2) + (0.0518P)^2 + 6.8961P]$ for Ce_2CuGa_{12} (90 K).

Table 2. Atomic Positions and Thermal Parameters

atom	Wyckoff position	x	y	z	occ.[a]	U_{eq} (Å^2)[b]
			La_2NiGa_{12}			
La	4*h*	3/4	1/4	0.24453(3)	1	0.00769(19)
Ni	2*c*	3/4	1/4	0	1	0.0081(4)
Ga1	4*g*	3/4	3/4	0.18023(6)	1	0.0091(3)
Ga2	4*g*	3/4	3/4	0.33936(6)	1	0.0117(3)
Ga3	8*m*	0.50037(9)	0.00037(9)	−0.08283(4)	1	0.0095(2)
Ga4	8*m*	0.56689(12)	0.06689(12)	0.42791(5)	1	0.0230(3)
			Ce_2NiGa_{12}			
Ce	4*h*	3/4	1/4	0.24439(4)	1	0.00734(19)
Ni	2*c*	3/4	1/4	0	1	0.0078(4)
Ga1	4*g*	3/4	3/4	0.18140(8)	1	0.0086(3)
Ga2	4*g*	3/4	3/4	0.33954(9)	1	0.0118(3)
Ga3	8*m*	0.50023(9)	0.00023(9)	−0.08340(5)	1	0.0092(2)
Ga4	8*m*	0.57024(12)	0.07024(12)	0.42816(7)	1	0.0211(3)
			La_2CuGa_{12}[c]			
La	4*h*	3/4	1/4	0.2463(2)	1	0.0090(8)
Cu	2*c*	3/4	1/4	0	1	0.0120(13)
Ga1	4*g*	3/4	3/4	0.1764(2)	1	0.0136(13)
Ga2	4*g*	3/4	3/4	0.3358(2)	1	0.0153(11)
Ga3	8*m*	0.5011(7)	0.0011(7)	−0.0845(2)	1	0.0151(7)
Ga4a	8*m*	0.567(4)	0.067(4)	0.4276(11)	0.42(4)	0.065(13)
Ga4b	8*m*	0.4471(21)	−0.0529(21)	0.4249(6)	0.60(4)	0.048(6)
			Ce_2CuGa_{12} (298 K)			
Ce	4*h*	3/4	1/4	0.24637(5)	1	0.0051(4)
Cu	2*c*	3/4	1/4	0	1	0.0101(7)
Ga1	4*g*	3/4	3/4	0.17753(12)	1	0.0075(5)
Ga2	4*g*	3/4	3/4	0.33633(12)	1	0.0104(5)
Ga3	8*m*	0.50036(14)	0.00036(14)	−0.08508(7)	1	0.0091(4)
Ga4	8*m*	0.5609(3)	0.0609(3)	0.42611(9)	1	0.0295(7)
			Ce_2CuGa_{12} (90 K)			
Ce	4*h*	3/4	1/4	0.24622(5)	1	0.0019(3)
Cu	2*c*	3/4	1/4	0	1	0.0035(6)
Ga1	4*g*	3/4	3/4	0.17778(11)	1	0.0032(4)
Ga2	4*g*	3/4	3/4	0.33677(11)	1	0.0042(4)
Ga3	8*m*	0.50017(13)	0.00017(13)	−0.08519(8)	1	0.0043(3)
Ga4	8*m*	0.56536(18)	0.06536(18)	0.42652(9)	1	0.0145(4)

[a] Occupancy of atoms. [b] U_{eq} is defined as one-third of the trace of the orthogonalized U_{ij} tensor. [c] Thermal parameters for La_2CuGa_{12} correspond to U_{11}.

Table 3. Selected Interatomic Distances (Å)

La_2NiGa_{12}		Ce_2NiGa_{12}	La_2CuGa_{12} (from NPD)		Ce_2CuGa_{12} (at 298 K)		Ce_2CuGa_{12} (at 90 K)
	La layer	Ce layer		La layer		Ce layer	Ce layer
Ln−Ga1 (×4)	3.1968(15)	3.1721(10)	La−Ga1 (×4)	3.270(1)	Ce−Ga1 (×4)	3.2321(16)	3.2211(12)
Ln−Ga2 (×4)	3.3755(14)	3.3593(11)	La−Ga2 (×4)	3.3805(17)	Ce−Ga4 (×4)	3.3526(16)	3.3471(13)
Ln−Ga4 (×2)	3.2560(13)	3.2363(17)	La−Ga4a (×2)	3.210(18)	Ce−Ga4 (×2)	3.2101(19)	3.1917(19)
Ln−Ga3 (×2)	3.3040(12)	3.2830(14)	La−Ga4b (×2)	3.241(14)	Ce−Ga3 (×2)	3.2863(16)	3.2768(17)
Ln−Ga3 (×2)	3.3081(12)	3.2855(14)	La−Ga3 (×2)	3.315(5)	Ce−Ga3 (×2)	3.2903(16)	3.2787(17)
			La−Ga3 (×2)	3.302(5)			

	$NiGa_{8/2}$segment	$NiGa_{8/2}$segment		$CuGa_{8/2}$segment		$CuGa_{8/2}$segment	$CuGa_{8/2}$segment
Ga1−Ga3 (×4)	2.6274(11)	2.6198(11)	Ga1−Ga3 (×4)	2.600(3)	Ga1−Ga3 (×4)	2.5854(14)	2.5798(13)
Ni−Ga3 (×4)	2.5010(12)	2.4936(10)	Cu−Ga3 (×4)	2.532(5)	Cu−Ga3 (×4)	2.5221(15)	2.5178(13)
Ni−Ga3 (×4)	2.5064(12)	2.4969(10)	Cu−Ga3 (×4)	2.549(6)	Cu−Ga3 (×4)	2.5274(15)	2.5203(13)

	Ga-only segment	Ga-only segment		Ga-only segment		Ga-only segment	Ga-only segment
Ga2−Ga4 (×4)	2.6144(12)	2.6080(12)	Ga2−Ga4a (×4)	2.665(14)	Ga2−Ga4 (×4)	2.6165(17)	2.6174(14)
Ga4−Ga4 (×1)	2.5189(17)	2.530(2)	Ga2−Ga4b (×4)	2.619(7)	Ga4−Ga4 (×1)	2.504(3)	2.521(3)
			Ga4a−Ga4a (×1)	2.517(34)			
			Ga4b−Ga4b (×1)	2.485(21)			

P4/nbm space group (No. 125, origin choice 2) with the Ce, *M* (*M* = Ni, Cu), Ga1, Ga2, Ga3 and Ga4 occupying the 4*h*, 2*c*, 4*g*, 4*g*, 8*m*, and 8*m* Wyckoff sites, respectively. This structure can be described as a repeating network of [*M*Ga] (*M* = Ni, Cu) units with Ce atoms occupying cavities made of Ga atoms, along the crystallographic *c*-axis. As shown in Table 3, in Ce_2MGa_{12} (*M* = Ni, Cu), the local Ce environment consists of Ce atoms, which are coordinated to 14 Ga atoms: 4 Ga1, 4 Ga2, 4 Ga3, and 2 Ga4. The Ce-centered Ga rectangular prism is capped by two Ga4 atoms and four Ga3 atoms. The Ce−Ga distances, which range from 3.1721(10) Å to 3.2903(16) Å, are in good agreement with typical Ce−Ga interatomic distances in other binary and ternary compounds such as $CeGa_2$, $CeGa_6$, Ce_3Ga, Ce_3Ga_2, Ce_5Ga_3, $CeNiGa_3$, $CeCu_2Ga_2$, and Ce_2PdGa_{12}.[5,20−25] The Ce−Ga4(×2) distances of 3.2101(19) Å in Ce_2CuGa_{12} are slightly shorter than the distances of 3.2363(17) Å found in Ce_2NiGa_{12}. However, the Ce−Ga1(×4) and Ce−Ga3(×2) distances of 3.2321(16) and 3.2903(16) Å, respectively, in Ce_2CuGa_{12} are slightly longer than Ce−Ga1(×4) and Ce−Ga3(×2) distances of 3.1721(10) Å and 3.2855(14) Å, respectively, in the Ni analogue.

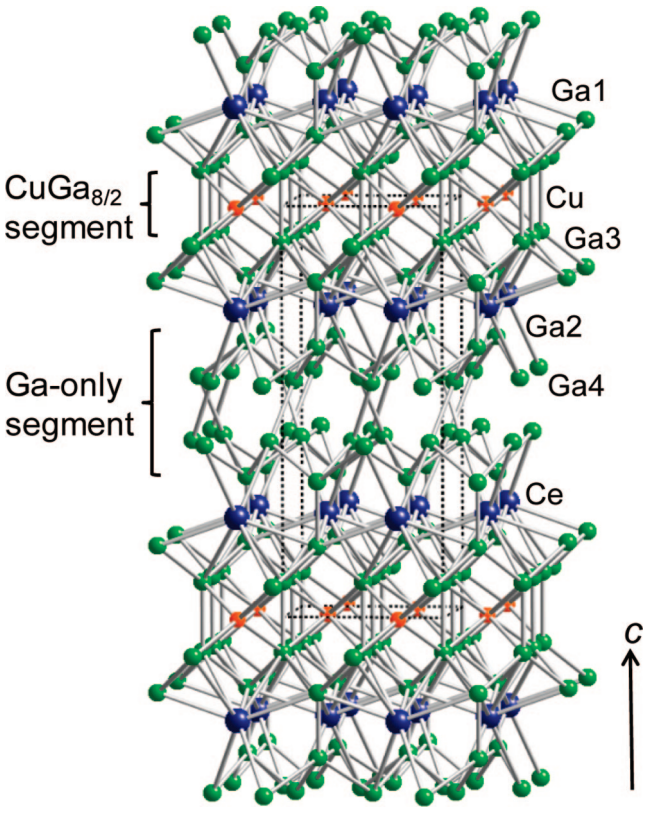

Figure 1. Crystal structure of Ce_2CuGa_{12} is shown along the *c*-axis, where the Ce atoms are represented with big blue spheres; the Cu atoms are denoted as orange spheres; and the Ga atoms are denoted with green spheres. Dashed lines are used to show the unit cell.

The [*M*Ga] (*M* = Ni, Cu) subunit is composed of edge sharing $MGa_{8/2}$ (*M* = Ni, Cu) rectangular prisms and Ga-only segments. In the rectangular prisms of Ce_2CuGa_{12}, Cu atoms are connected to four Ga3 atoms with interatomic distances of 2.522(2) Å and four additional Ga3 atoms by 2.527(2) Å, which are slightly longer than the Ni−Ga distances of 2.494(1) Å and 2.497(1) Å in Ce_2NiGa_{12}. These distances are also in good agreement with typical of *M*−Ga (*M* = Ni, Cu) bonds in other binary and ternary compounds such as Ni_2Ga, Ni_3Ga, $CuGa_2$, Cu_9Ga_4, $CeNiGa_3$, Ce_2NiGa_{10}, and $CeCu_2Ga_2$.[24−29] The Ga1−Ga3 interatomic distance of 2.585(1) Å found in the $CuGa_{8/2}$ rectangular prisms have shorter contacts than the Ga1−Ga3 distance of 2.620(1) Å in the $NiGa_{8/2}$ rectangular prisms of Ce_2NiGa_{12} along the *c*-axis.

(20) Kimmel, G.; Dayan, D.; Grill, A.; Pelleg, J. *J. Less-Common Met.* **1980**, *75*, 133–140.
(21) Yatsenko, S. P.; Semyannikov, A. A.; Semenov, B. G.; Chuntonov, K. A. *J. Less-Common Met.* **1979**, *64*, 185–199.
(22) Dayan, D.; Pelleg, J.; Guisser, R. *J. Less-Common Met.* **1979**, *68*, 199–205.
(23) Dzyana, D. I.; Gladishevs'kii, E. I.; Krip'yakevich, P. I. *Dopov. Akad. Nauk Ukr. RSR, Ser. A* **1968**, *30*, 282–284.
(24) Nicklas, M.; Moreno, N. O.; Borges, H. A.; Bauer, E. D.; Sarrao, J. L.; Thompson, J. D. *J. Magn. Magn. Mater* **2004**, *272−276*, E111–E112.
(25) Grin, Y. N. *Dopov. Akad. Nauk Ukr. RSR, Ser. A* **1982**, *7*, 6–9.
(26) El-Boragy, M.; Schubert, K. *Z. Metallkd.* **1972**, *63*, 52–53.
(27) Stokhuyzen, R.; Brandon, J. K.; Chibh, P. C.; Pearson, W. B. *Acta Crystallogr., Sect. B: Struct. Sci.* **1974**, *B30*, 2910–2911.
(28) Feschotte, P.; Eggimann, P. *J. Less-Common Met.* **1979**, *63*, 15–30.
(29) Yarmolyuk, Y. P.; Grin, Y. N.; Rozhdestvenskaya, I. V.; Usov, O. A.; Kuz'min, A. M.; Bruskov, V. A.; Gladyshevskii, E. I. *Kristallografiya* **1982**, *27*, 999–1001.

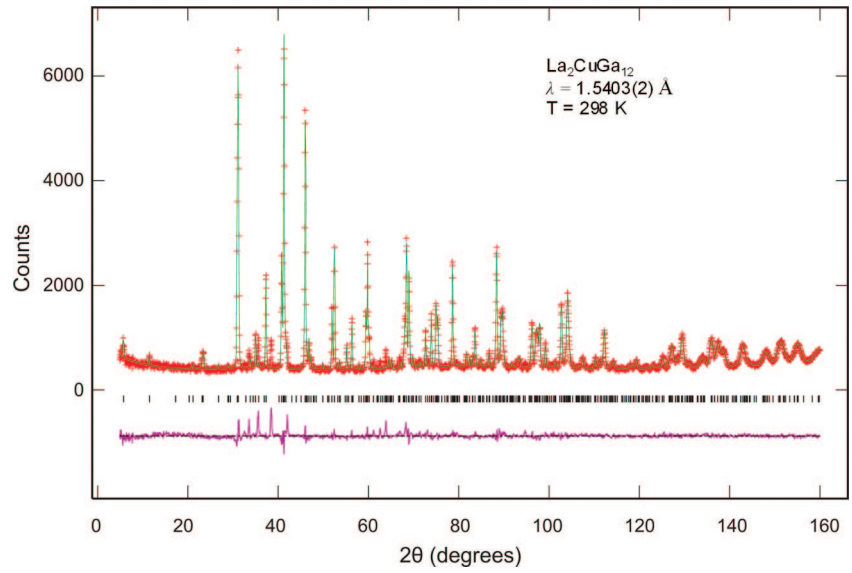

Figure 2. Neutron powder diffraction data for La_2CuGa_{12} is shown with red crosses. Rietveld refinement fits and the difference curve are shown in green and magenta, respectively. Calculated reflections are marked with black tick marks.

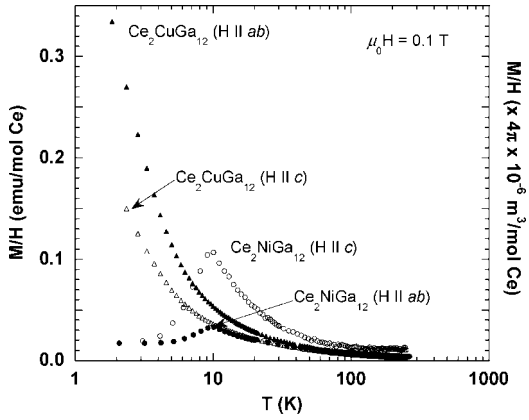

Figure 3. Magnetic susceptibility (emu/mol Ce) of Ce_2MGa_{12} (M = Ni, Cu) as a function of temperature is shown. Closed and open markers represent data collected with field parallel and perpendicular to the crystallographic c-axis of Ce_2MGa_{12} (M = Ni, Cu), respectively. Error bars represent (±) the standard uncertainty of each measurements.

The Ga-only segment of the [MGa] (M = Ni, Cu) subunit has two different Ga layers which consist of Ga2 and Ga4 atoms. Within the Ga2 layer for both compounds, Ga−Ga interatomic distances along the *ab*-plane range from 4.268 to 6.108 Å, which are too far to be considered bonding when compared with the covalent radii of 2.50 Å observed for Ga−Ga bonds. The Ga4−Ga4 interatomic distances of 3.135 Å and 3.143 Å for Ce_2NiGa_{12} and Ce_2CuGa_{12}, respectively, along the *ab*-plane are also far from typical bond lengths of Ga−Ga and the sum of Ga covalent radii (2.50 Å).[30] However, the Ga4−Ga4 interatomic distances along the *c*-axis are 2.530(2) Å and 2.504(3) Å for Ce_2NiGa_{12} and Ce_2CuGa_{12}, respectively, which are very close to the sum of Ga covalent radii (2.50 Å).[30] In addition, Ga4 atoms are connected by distances of 2.608(1) Å (Ce_2NiGa_{12}) and 2.617(2) Å (Ce_2CuGa_{12}) with Ga2 atoms along the *c*-axis, which are also in good agreement with the typical interatomic distances in Ga containing binaries such as $CeGa_2$, $CeGa_6$.[20]

From our observation of the difference Fourier syntheses for La_2NiGa_{12} and Ce_2MGa_{12} (M = Ni, Cu), another 8*m* Wyckoff site, which is close to the Ga4 position, has been identified. In addition, single crystal X-ray data show an anomalous behavior of the displacement parameters for the Ga4 position, which has its ellipsoid elongated in the *ab*-direction. The former and latter observations may be indicative of statistical and dynamic disorder in the structures, respectively. To examine whether dynamic disorder was present in the structure of Ce_2CuGa_{12}, we collected single crystal X-ray data for Ce_2CuGa_{12} at 90 K as shown in Tables 1–3. However, the Ga4 atom still shows a large displacement parameter at T = 90 K, implying that a dynamic disorder does not play an important role in this structure. After consideration of that result, a statistical disorder for the Ga4 position was carefully checked. The refinement of partially occupied atoms in two sites, however, did not greatly affect the displacement parameter for Ga4 position nor the other statistical values, such as R factor. Therefore, although there might be disorder in the Ln_2MGa_{12} (Ln = La, Ce; M = Ni, Cu) compounds, we were not able to model the disorder satisfactorily using single crystal X-ray diffraction experiments.

Neutron Powder Diffraction. The structure of La_2CuGa_{12} was refined using neutron powder diffraction techniques. The

Table 4. Magnetic Properties of Ce_2MGa_{12} (M = Ni and Cu)

	C	θ (K)	χ_0 (× 10^{-5} emu/mol) (× 4π × 10^{-6} m^3/mol)[a]	μ_{calcd} (μ_B) (× 9.27 × 10^{-24} Am^2)[a]	μ_{eff} (μ_B)	fit range (K)	ordering T_N (K)
Ce_2NiGa_{12}	0.62	−6.67	5.60	2.54	2.23	20−200	10 K (H ∥ *c*)
	0.67	−16.97	0.12	2.54	2.31	20−200	10 K (H ∥ *ab*)
Ce_2CuGa_{12}	0.65	−11.04	0.06	2.54	2.28	20−200	−(H ∥ *c*)
	0.75	−5.88	0.38	2.54	2.45	20−200	−(H ∥ *ab*)

[a] SI units.

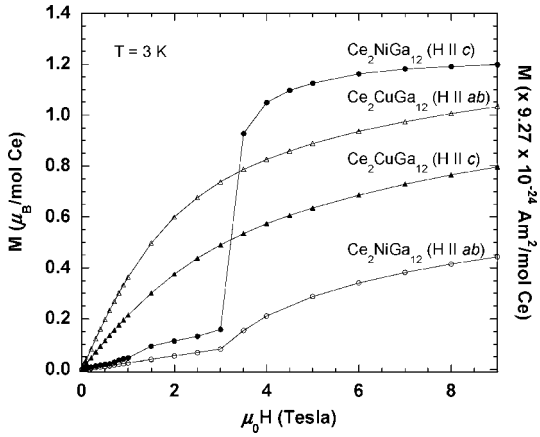

Figure 4. Magnetization of Ce_2MGa_{12} (M = Ni, Cu) as a function of magnetic field at 3K is shown. Closed and open markers represent data collected with field parallel and perpendicular to the crystallographic c-axis of Ce_2MGa_{12} (M = Ni, Cu), respectively.

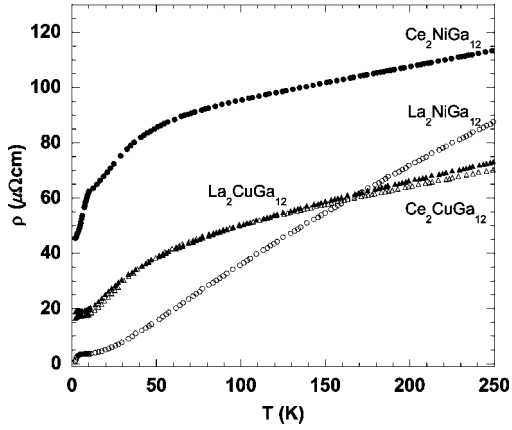

Figure 5. Normalized electrical resistivity of Ln_2MGa_{12} (Ln = La, Ce; M = Ni, Cu) as a function of temperature for current parallel to the *ab*-plane is shown.

NPD fit for La_2CuGa_{12} is shown in Figure 2. The background was fit using a 13-term shifted Chebychev polynomial. The lattice parameters, zero point, and scale factor were also refined. The peak profile was modeled using Gaussian and Lorentzian terms. The structure of Ce_2CuGa_{12} was used as an initial structural model and reasonable isotropic atomic displacement parameters were constrained for the initial least-squares cycle. However, upon refinement elongation of the atomic displacement ellipsoid for the Ga4 atom (8*m* Wyckoff site) was observed. The model was refined for statistical disorder, and an additional Ga atom, which is referred to as Ga4b, was added to the structural model on the 8*m* site. The original Ga4 atom, which exists in the parent and analogous phases, has been assigned the label Ga4a for clarity in the La_2CuGa_{12} phase. The Ga4a and Ga4b atoms were observed to have partial occupancies of 0.42(4) and 0.60(4), respectively, which confirms the stoichiometry of La_2CuGa_{12}. The occupancies of the La, Cu, Ga1, Ga2, and Ga3 atoms were allowed to refine freely, but the occupancies remained close to unity, suggesting full occupancy on these particular sites. The atomic displacement parameters were refined anisotropically for all atoms. This sample was also observed to contain $\approx$ 5% of an unknown impurity phase. This impurity phase was not observed to be consistent with any other known binary, ternary, or oxide combinations of the starting elements.

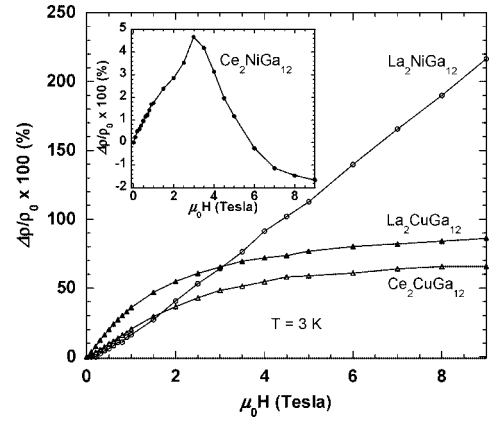

Figure 6. MR % of Ln_2MGa_{12} (Ln = La, Ce; M = Ni, Cu) as a function of field at 3 K is shown. The inset shows MR % of Ce_2NiGa_{12} for clarity.

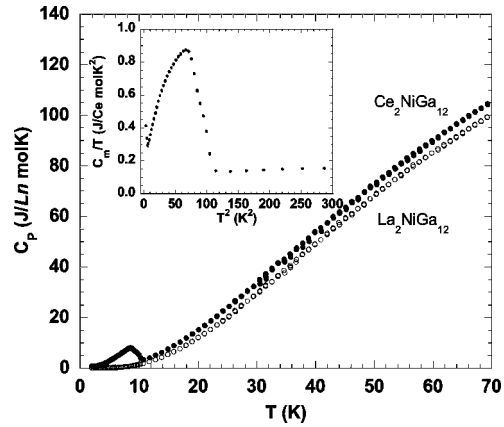

Figure 7. Specific heat of Ln_2NiGa_{12} (Ln = La, Ce) as a function of temperature. The inset shows C_m/T versus T^2 for Ce_2NiGa_{12} after subtracting lattice contribution.

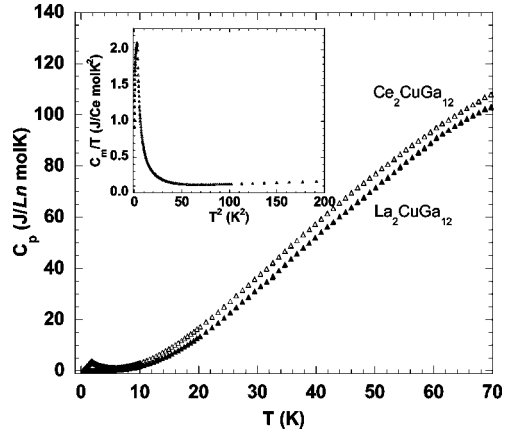

Figure 8. Specific heat of Ln_2CuGa_{12} (Ln = La, Ce) as a function of temperature. The inset shows C_m/T versus T^2 for Ce_2CuGa_{12} after subtracting lattice contribution.

Physical Properties. Temperature-dependent magnetic susceptibility of single crystals of Ce_2MGa_{12} (M = Ni, Cu) is shown in Figure 3. An external magnetic field (μ_0H) of 0.1 T was applied along both the c-axis and the *ab*-plane of the crystal. A downturn in the magnetic susceptibility data

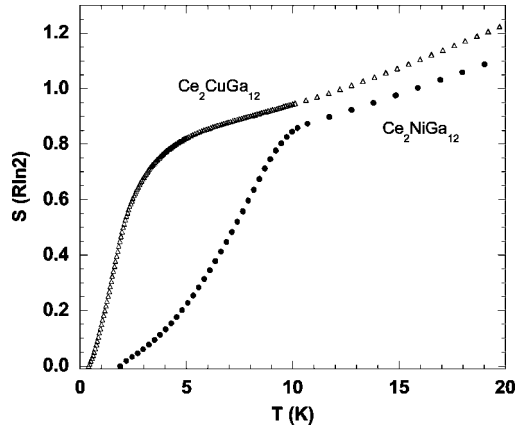

Figure 9. The magnetic entropy of Ce_2MGa_{12} (M = Ni, Cu) as a function of temperature.

for both directions of Ce_2NiGa_{12} suggests antiferromagnetic long-range order at $T_N = 10$ K for both directions. In contrast, Ce_2CuGa_{12} does not magnetically order down to 2 K. The inverse magnetic susceptibility was fit from 20 to 200 K and is not shown here. From this linear fit, the effective moments, μ_{eff}, of Ce_2NiGa_{12} are 2.23 μ_B (2.07×10^{-23} Am^2/Ce) for H ∥ c-axis and 2.31 μ_B (2.14×10^{-23} Am^2/Ce) for H ∥ ab-plane, which are smaller than but close to the calculated Ce^{3+} moment, $\mu_{eff} = 2.54$ μ_B (2.36×10^{-23} Am^2), with $\theta = -6.67$ K (H ∥ c-axis) and -16.97 K (H ∥ ab-plane). A modified Curie−Weiss law: $\chi = \chi_0 + C/(T - \theta)$, was used to fit the data, where χ_0 represents the temperature-independent term, C is the Curie constant, and θ is the Weiss temperature. This result is consistent with Ce-moment antiferromagnetism for Ce_2NiGa_{12}. Also, the effective moments of 2.28 μ_B (2.11×10^{-23} Am^2) for H ∥ c-axis and 2.45 μ_B (2.27×10^{-23} Am^2) for H ∥ ab-plane for Ce_2CuGa_{12} are observed with the Weiss temperatures of −11.04 K (H ∥ c-axis) and − 5.88 K (H ∥ ab-plane) by using the same equation. The magnetic properties of Ce_2MGa_{12} (M = Ni, Cu) are summarized in Table 4.

Figure 4 shows isothermal magnetization data as a function of an external magnetic field with the crystal aligned along the c-axis and ab-plane up to the field ($\mu_0 H$) of 9 T at 3 K. For Ce_2NiGa_{12}, the experimental saturation is smaller than the calculated μ_{sat} of 2.14 μ_B (1.98×10^{-23} Am^2) for Ce^{3+}. The magnetization of Ce_2NiGa_{12} linearly increases at low fields consistent with antiferromagnetism. However, the data of Ce_2NiGa_{12} above 3 T show a jump indicating a transition at ∼3 T. This is likely a spin-flop transition. The magnetization displays paramagnetic behavior above the spin-flop transition. As the magnetic field increases, the magnetization of Ce_2CuGa_{12} increases, consistent with a paramagnet. However, above 2 T, the magnetization of Ce_2CuGa_{12} begins to saturate at 0.80 μ_B (7.42×10^{-24} Am^2) along the c-axis.

Figure 5 shows the electrical resistivity of single crystals of Ln_2MGa_{12} (Ln = La, Ce; M = Ni, Cu) as a function of temperature in the ab-plane, where each compound shows metallic behavior with RRR (residual resistivity ratio) values of 98, 2.6, 4.1, and 4.5 for La_2NiGa_{12}, Ce_2NiGa_{12}, La_2CuGa_{12}, and Ce_2CuGa_{12}, respectively. The onset of a broad shoulder for Ce_2NiGa_{12}, which may be indicative of Kondo coherence, is observed in the resistivity below 100 K. A kink in the resistivity of Ce_2NiGa_{12} is observed at 10 K, which coincides with the magnetic ordering temperature and indicates a decrease in the spin disorder scattering. However, the resistivity of La_2CuGa_{12} and Ce_2CuGa_{12} are similar and there is no indication of Kondo coherence in the Ce compound.

Figure 6 shows the magnetoresistance (MR % = $(\rho_H - \rho_0)/\rho_0 \times 100$) of single crystals of Ln_2MGa_{12} (Ln = La, Ce; M = Ni, Cu) at 3 K as a function of field in the ab-plane. The Ln_2MGa_{12} (Ln = La, Ce; M = Ni, Ce) compounds except Ce_2NiGa_{12} show large positive magnetoresistance, with ratios up to 216, 86, and 65% at the field ($\mu_0 H$) of 9 T for La_2NiGa_{12}, La_2CuGa_{12}, and Ce_2CuGa_{12}, respectively. These values are much larger than MR < 10%, which are typically found for most intermetallic compounds at low temperatures. This large positive magnetoresistance for Ce_2CuGa_{12} may be due to classical magnetoresistance; however it is considerably larger than typical intermetallics. The MR of La_2CuGa_{12} and Ce_2CuGa_{12} are similar. Based on the resistivity and magnetoresistance data, the Ce moments are decoupled from the conduction electrons in Ce_2CuGa_{12}. The MR of La_2NiGa_{12} is linear and does not show signs of saturation. There have been several recent discoveries of a large nonsaturating MR in low carrier density nonmagnetic metals and semiconductors.[31−36] This effect is usually attributed to a change in the structural symmetry involving a possible transition to a charge density wave (CDW) state[37] or high-field quantization effects.[31] However, there is no evidence for CDW in the transport. As such, the large linear MR in La_2NiGa_{12} warrants further investigation, and future work will focus on measuring the MR at higher fields. The MR of the Ce_2NiGa_{12} shows a rather sharp maximum ∼3 T, coinciding with the metamagnetic transition as shown in the inset of Figure 6.

The specific heat of Ln_2NiGa_{12} (Ln = La, Ce) is shown in Figure 7. A big jump up to 8 J mol^{-1} K^{-1} for Ce_2NiGa_{12} is consistent with its ordering temperature ($T_N \approx 10$ K) observed in the magnetic susceptibility data (See Figure 3). As shown in the inset of Figure 7, after subtracting the phonon contribution to the heat capacity a $\gamma \approx 191$ mJ mol^{-1} K^{-2} is obtained, which indicates that Ce_2NiGa_{12} exhibits heavy-fermion behavior. Below the transition, γ decreases to 2.4 K and then shows an upturn to the lowest temperature. The gamma value remains large ($\gamma \approx 411$ mJ mol^{-1} K^{-2}) at the lowest temperature. Figure 8 shows the specific heat of Ln_2CuGa_{12} (Ln = La, Ce). Although there is no evidence of a magnetic transition for Ce_2CuGa_{12} in the magnetic susceptibility data, the specific heat of Ce_2CuGa_{12} shows a sharp peak of ∼3.8 J mol^{-1} K^{-1} at ∼1.8 K, which corresponds to a second-order magnetic transition which is not within the range of our susceptibility data. The Weiss

(30) Emsley, J. *The Elements*; 3rd ed.; Oxford University Press: New York, 1998.
(31) Abrikosov, A. A. *Phys. Rev. B: Condens. Matter* **1999**, *60*, 4231–4234.
(32) Lifshits, I. M.; Peshanskii, V. G. *Sov. Phys. JETP* **1959**, *8*, 875.
(33) Falicov, L. M.; Smith, H. *Phys. Rev. Lett.* **1972**, *29*, 124–127.
(34) Soule, D. E. *Phys. Rev.* **1958**, *112*, 698–707.
(35) Butko, V. Y.; DiTusa, J. F.; Adams, P. W. *Phys. Rev. Lett.* **2000**, *85*, 162–165.
(36) Young, D. P.; Goodrich, R. G.; DiTusa, J. F.; Guo, S.; Adams, P. W.; Chan, J. Y.; Hall, D. *Appl. Phys. Lett.* **2003**, *82*, 3713–3715.
(37) Overhauser, A. W. *Phys. Rev. B* **1971**, *3*, 3173–3182.

temperatures along both crystallographic directions of Ce_2CuGa_{12} are negative, suggesting the transition observed in the specific heat is a bulk antiferromagnetic transition. To estimate the electronic contribution of the total heat capacity, the heat capacity of Ce_2CuGa_{12} as C/T versus T^2 is plotted in inset of Figure 8. The value of γ above the transition is 69 mJ mol^{-1} K^{-2}, which indicates that the compound is a moderate heavy-fermion. Below the transition, at the lowest temperature, $T = 0.4$ K, gamma remains large $\approx$ 900 mJ mol^{-1} K^{-2}. Integrating C/T over T gives the entropy (see Figure 9), which increases with temperature and almost saturates above the transition temperatures, reaching the value of $0.87R\ln 2$ and $0.8R\ln 2$ for Ce_2NiGa_{12} and Ce_2CuGa_{12}, respectively. This suggests that the magnetic ground-state is a doublet for both compounds. The fact that the entropy does not recover the full $R\ln 2$ above the transition temperature might indicate the presence of the Kondo effect or mixed valence among the Ce ions, although the susceptibility data almost recovers the full Hund's rule moment for Ce^{3+}. Below 10 K, the electrical resistivity of Ce_2NiGa_{12} and Ce_2CuGa_{12} is proportional to T^2, indicating Fermi liquid behavior. The Kadowaki−Woods ratio (A/γ^2), where A represents the coefficient of the quadratic term in the temperature-dependent resistivity and γ is the coefficient of the linear term in the temperature-dependent specific heat, has values of $\sim 5.7 \times 10^{-6}$ and $\sim 8.3 \times 10^{-6}$ for Ce_2NiGa_{12} and Ce_2CuGa_{12}, respectively, which are close to what one would expect for heavy-fermion behavior.

In our previous work, we have suggested that the higher magnetic ordering temperature ($T_N = 11$ K) in Ce_2PdGa_{12} compared to $CePdGa_6$ may be attributed to increased hybridization between the Ce 4*f* electrons and conduction electrons (Ga), where the higher Ga contacts can contribute additional carriers to the magnetic Ce^{3+} ion.[5] Another factor involves the number of *d* electrons, which can be changed by substituting different transition metals M (M = Ni, Pd) to M = Cu in Ce_2MGa_{12}. Substitution of M = Ni, Pd to Cu results in the change in the number of carriers. The evidence for a Kondo resonance found in the Ce_2NiGa_{12} is not found in the Ce_2CuGa_{12} sample, and this is evident in the transport data where the resistivity of the La_2CuGa_{12} is essentially the same with the Ce_2CuGa_{12} analog. Furthermore, the MR of the La_2CuGa_{12} and Ce_2CuGa_{12} is similar as well. Also, the Ce and La analogs with Ni show a linear MR with fields ($\mu_0 H$) up to 3 T before the Ce undergoes a magnetic transition.

Acknowledgment. J.Y.C. acknowledges an NSF-CAREER award (Grant DMR0237664) and Alfred P. Sloan Fellowship for partial support of this project. D.P.Y. acknowledges an NSF-CAREER award (Grant DMR0449022). Work at the Brookhaven National Laboratory was carried out under the auspices of the U.S. Department of Energy. We also acknowledge Dr. Frank Fronczek and Judith K. Stalick for useful discussion. Certain trade names and company products are identified in order to specify adequately the experimental procedure. In no case does such identification imply recommendation or endorsement by the National Institute of Standards and Technology, nor does it imply that the products are necessarily the best for the purpose.

Supporting Information Available: Additional crystallographic data in CIF format. This material is available free of charge via the Internet at http://pubs.acs.org.

CM801693T